Available online at www.sciencedirect.com
SCIENCE DIRECT®
Journal of Solid State Chemistry 179 (2006) 2616–2628
JOURNAL OF SOLID STATE CHEMISTRY
www.elsevier.com/locate/jssc

Na–Li–$[V_3O_8]$ insertion electrodes: Structures and diffusion pathways

Michael Schindler[a,*], Frank C. Hawthorne[c], Malcolm A. Alexander[a], Rory A. Kutluoglu[a,1], Petre Mandaliev[b], Norman M. Halden[c], Roger H. Mitchell[a]

[a]*Department of Geology, Lakehead University, Thunder Bay, Ont., Canada P7B 5E1*
[b]*Laboratory for Waste Management, Paul Scherrer Institute, CH-5232 Villigen PSI, Switzerland*
[c]*Department of Geological Sciences, University of Manitoba, Winnipeg, Man., Canada R3T 2N2*

Received 20 April 2006; received in revised form 11 May 2006; accepted 12 May 2006
Available online 19 May 2006

Abstract

The potential insertion-electrode compounds $Na_{1.2}[V_3O_8]$ (NaV) and $Na_{0.7}Li_{0.7}[V_3O_8]$ (NaLiV) were synthesized from mixtures of Na_2CO_3, Li_2CO_3 and V_2O_5, which were melted at 750° and subsequently cooled to room temperature. The structures of NaV and LiV contain sheets of polymerized (VO_n) polyhedra, which are topologically identical to the sheet of polymerized polyhedra in $Li_{1.2}[V_3O_8]$ (LiV). Vanadium occurs in three different coordination environments: [2 + 3] V(1), [2 + 2 + 2] V(2) and [1 + 4 + 1] V(3). Calculated bond-valence sums indicate that V^{4+} occurs preferentially at the V(3) site, which agrees with the general observation that [6]-coordinated V^{4+} prefers [1 + 4 + 1]-rather than [2 + 2 + 2]-coordination. The *M*-cations Na and Li occur at three distinct sites, *M*(1), *M*(2) and *M*(3) between the vanadate sheets. The *M*(1)-site is fully occupied and has octahedral coordination. The *M*(2) sites are partly occupied in NaV and NaLiV, in which they occur in [4]- and [6]-coordination, respectively. Li partly occupies the *M*(3) site in NaLiV, in which it occurs in [3]-coordination. The *M*(2) and *M*(3) sites in NaLiV occur closer to the vanadate sheets than the *M*(2) sites in NaV and LiV. The shift in these cation positions is a result of the larger distance between the vanadate sheets in NaLiV than in LiV, which forces interstitial Li to move toward one of the vanadate sheets to satisfy its coordination requirements. Bond-valence maps for the interstitial cations Na and Li are presented for NaV, NaLiV and LiV. These maps are used to determine other potential cation positions in the interlayer and to map the regions of the structure where the Na and Li have their bond-valence requirements satisfied. These regions are potential pathways for Na and Li diffusion in these structures, and are used to explain chemical diffusion properties of Na and Li in the Na–Li–$[V_3O_8]$ compounds.
© 2006 Elsevier Inc. All rights reserved.

Keywords: Alkali insertion electrodes; Vanadate; Structure; Bond-valence maps; Diffusion pathways

1. Introduction

The vanadium bronze $Li_{1+x}[V_3O_8]$ is one of several vanadium oxides that have received attention as an insertion electrode for rechargeable lithium batteries [1–9]. The major structural property of this compound is its ability to accommodate a maximum of three additional Li^+ ions per formula unit without major disturbance of the structural features of the vanadate layer. The reversible intercalation-removal process of Li is charge-balanced by reduction–oxidation of V^{5+}–V^{4+} in the vanadate layer [10]. The presence of other alkali metals in the isostructural $M_{1+x}[V_3O_8]$ (M = Na or *K*) compounds produces interlayer distances between the vanadate sheets that are larger than in $Li_{1+x}[V_3O_8]$ [11,12]. These $M_{1+x}[V_3O_8]$ phases have also been tested as positive electrodes for sodium and magnesium batteries [13,14]. Kumagai et al. [9] examined the $Li_{1-x}Na[V_3O_8]$ solid solution as a positive material for secondary lithium batteries. Here, $Li_{0.7}Na_{0.3}[V_3O_8]$ showed the best electrochemical performance among several $Li_{1-x}Na[V_3O_8]$ compounds. This observation was attributed to a higher chemical diffusion coefficient of the interstitial cations, possibly as a result of a larger interlayer spacing between the vanadate sheets.

*Corresponding author. Present address: Department of Geological Sciences, University of Manitoba, Winnipeg, Man., Canada.
Fax: 204 474 7623.
E-mail address: schindl0@cc.umanitoba.ca (M. Schindler).
[1]Present address: Aeroquest Ltd., 4-845 Main St. E., Milton, Ont., Canada L9T 3Z3.

0022-4596/$ - see front matter © 2006 Elsevier Inc. All rights reserved.
doi:10.1016/j.jssc.2006.05.009

The structure of $Li_{1+x}[V_3O_8]$ was first described by Wadsley [15] ($x>0.0$) and later refined by de Picciotto et al. [10] (for $x=0.2$). The structure is monoclinic ($P2_1/m$) and is composed of vanadate sheets with V in [5] and [6]-coordination (Fig. 1a). De Picciotto et al. [10] showed that Li fully occupies the octahedrally coordinated $M(1)$ site and partly occupies the tetrahedrally coordinated $M(2)$ site. Furthermore, they reported the structure of $Li_4[V_3^{4+}O_8]$, an end-product of a lithiation process of $Li_{1.2}[V_3O_8]$ (short: LiV), in which all Li cations occupy octahedrally coordinated sites in the interlayer. Using unit-cell parameters determined from X-ray diffraction photos, Wadsley [15] predicted that $Na_{1+x}[V_3O_8]$ is isostructural with $Li_{1+x}[V_3O_8]$, and Kumagai et al. [9] reported complete solid-solution between $Na[V_3O_8]$ and $Li[V_3O_8]$. Despite their interesting electrochemical properties, details of the structures of $Na_{1+x}[V_3O_8]$ and phases of the $Na_xLi_y[V_3O_8]$ solid-solution have not been reported. As part of our general interest in vanadate structures [16–20], we have synthesized phases of the $Na_xLi_y[V_3O_8]$ solid-solution and describe here the structures of $Na_{1.2}[V_3O_8]$ (short: NaV) and $Na_{0.7}Li_{0.7}[V_3O_8]$ (short: NaLiV).

Furthermore, we present in the second part of the paper bond-valence maps with respect to the interstitial cations Na and Li for the structures of NaLiV, NaV and LiV. These maps will be used to calculate other potential Na and Li positions and to determine possible diffusion pathways in these structures.

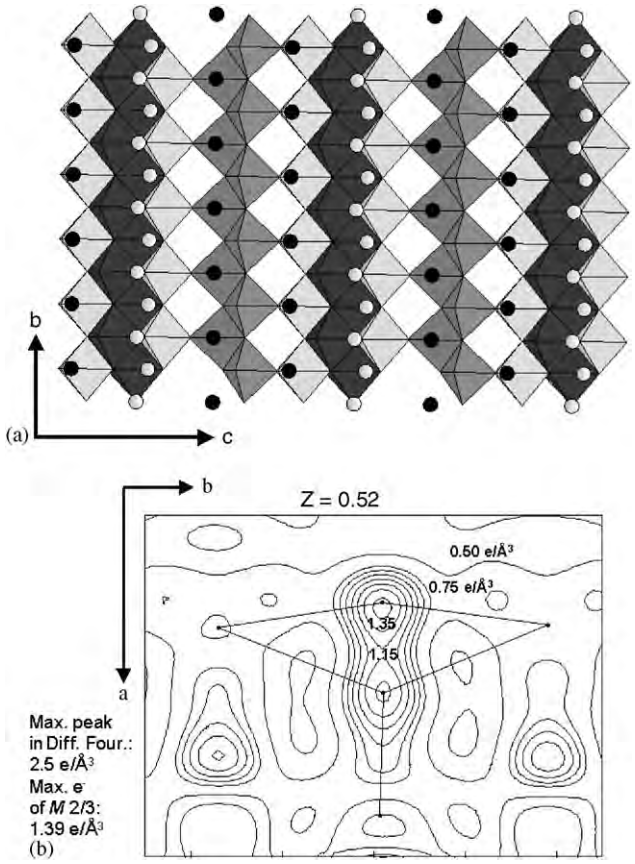

Fig. 1. (a) Parts of the vanadate layer in the structures of NaV, LiV and NaLiV, indicating the tetravanadate chain in light grey (V(2) dipyramid) and black (V(3) dipyramid) and the divanadate chain in grey. (b) Difference-Fourier map in the a–b plane of NaLiV, indicating two electron-density peaks 1.02 Å apart in the vicinity of the $M(2)$ site. Also shown are the positions of the O(5) atoms and the $M(2)$–O(5) and $M(3)$–O(5) bonds and the electrons per cubic Angstrom [$e^-/Å^3$] at the contour lines.

2. Experimental

2.1. Synthesis and X-ray powder diffraction

Single crystals of NaV and NaLiV were prepared after the procedure of Wadsley [15] by mixing Na_2CO_3, Li_2CO_3 and V_2O_5 in the molar ratios 1:0:2 and 0.5:0.5:2, respectively. The samples were heated in open quartz capillaries at 750 °C for 24 h, and then subsequently cooled at a rate of 1 °C/min in a Lindberg/Blue Mini-Mite Tube furnace. The synthesis products were identified with a Phillips PW 1820 powder diffractometer. Major phases of the final products are non-consumed V_2O_5 and black fibrous bundles of either NaV or NaLiV.

2.2. Single-crystal X-ray diffraction data collection

Suitable crystals of NaV and NaLiV were mounted on a Bruker P4 diffractometer fitted with an APEX CCD detector at a crystal-to-detector distance of 5.025 cm. A sphere of three-dimensional data was collected for each crystal using Mo$K\alpha$ radiation and frame widths of 0.2° in ω with count times per frame of 30s (NaV) and 45s (NaLiV). An empirical absorption correction (SADABS [21]) was applied. The unit cells were refined with 4502 reflections for NaV and 3716 reflections for NaLiV. Systematic absences for both compounds are consistent with space group $P2_1/m$. Details of the X-ray data collection and structure refinement are given in Table 1.

2.3. Structure refinements

Scattering factors for neutral atoms were taken from the International Tables for X-ray Crystallography [22]. The SHELXTL-97 version [23] was used for refinement of the crystal structures.

The structure of $Li_{1.2}[V_3O_8]$ [10] was used as a starting model for refinement of the structures of NaV and NaLiV. Refinement of NaV converged after several least-square cycles with a final R_1-value of 4.3% (Table 1). In the structure refinement of NaLiV, we used scattering factors for Na and Li for refinement of the site occupancies of the $M(1)$ and $M(2)$ sites, respectively. Refinement of the isotropic-displacement factor at the $M(2)$ site gave a large U_{iso} value of 0.09 Å^2. Difference-Fourier maps at $z=0.52$ in the vicinity of the $M(2)$ site showed two electron-density maxima 1.02 Å apart with heights of 1.39 and 1.27 $e^-/Å^3$, respectively (Fig. 1b, note that the maximum peak in the

difference Fourier map has a height of 2.5 $e^-/Å^3$). These peaks suggest splitting of the $M(2)$ site into $M(2)$ and $M(3)$ sites. For both sites, the occupancies were refined using the neutral scattering factor for Li and their isotropic-displacement factors were constrained to be equal. After splitting the $M(2)$ site, refinement of the NaLiV structure converged to a final R_1-value of 5.6% (Table 1). Final atom positions and displacement factors are listed in Table 2 and selected bond-lengths are given in Table 3. Table 4 lists the average M–O bond-lengths and the assigned site-occupancies at each M site.

Table 1
Crystallographic data and refinement parameters

Compound	$Na_{1.2}[V_3O_8]$	$Na_{0.7}Li_{0.7}[V_3O_8]$
a (Å)	7.3316(7)	7.101(2)
b	3.6070(4)	3.6106(9)
c	12.139(1)	12.097(3)
β (deg)	107.368(2)	106.601(5)
V(Å^3)	*306.38*	*297.21*
Space group	$P2_1/m$	$P2_1/m$
Z	1	1
μ(mm^{-1})	4.57	4.66
D_{calc} (g/cm^3)	3.343	3.339
Size (mm)	0.20 × 0.03 × 0.02	0.25 × 0.02 × 0.01
Radiation	Mo$K\alpha$/Gr	Mo$K\alpha$/Gr
No. of reflections	4502	3716
No. in Ewald sphere	2644	2628
No. unique	475	461
No. $\lvert F_o\rvert > 4\sigma(\lvert F_o\rvert)$	432	422
R_{merge} %	2.27	2.71
Range of h	−9 to 9	−9 to 9
Range of k	−5 to 4	−5 to 4
Range of l	−17 to 17	−16 to 16
$R_1(\lvert F_o\rvert > 4\sigma)$ %	4.28	5.56
$wR_2(F_o^2)$ %	11.12	13.28
Weighting a	0.0564	0.0512

$R_1 = 3(\lvert F_o\rvert - \lvert F_c\rvert)/3\lvert F_o\rvert \times 100$.
$wR_2 = [\sum[w(F_o^2 - F_c^2)^2/\sum w(F_o^2)^2]]^{0.5}$,
$w = 1/[\sigma^2(F_o^2) + (a \times P)^2]$; $P = 1/3$ Max $(0, F_o^2) + 2/3 \times F_c^2$.

2.4. Chemical analysis: electron microprobe and laser-ablation inductively couple plasma mass spectroscopy (LA-ICP-MS)

The chemical composition of a crystal from the NaV-sample (not the crystal of the X-ray diffraction experiment) was analysed with a Cameca SX-50 electron microprobe operating in wavelength-dispersion mode with an accelerating voltage of 15 kV and a specimen current of 20 nA. The standards were albite, $NaAlSi_3O_8$ for Na and VP_2O_7 for V. The measured chemical composition of the crystal was $Na_{1.2}[V_3O_8]$, and this was used as an internal standard for vanadium in the ICP-MS analysis.

^{7}Li, ^{23}Na and ^{51}V were measured using an Element2 ICP-MS and a Merchantek LUV 213 laser. Vanadium was determined independently by electron microprobe and was used as an internal standard. The external calibration standard was NIST glass 610, using the nominal values reported by Pearce et al. [32]. The choice of isotopes was constrained by expectations of sensitivity as well as the potential for spectral overlap and molecular interference. Operating in low-resolution mode, $^7Li^{16}O$ will interfere with ^{23}Na; oxide production was minimized by tuning conditions to less than 3% of the count rate of the interfering isotope. Measured element intensities were processed using GLITTER [33]. Standard signals were averaged, and local backgrounds were used on all signals. The parts of the sample spectra selected were chosen to keep fractionation below 10% and the fractionation-to-error ratio at or below 3.

Table 2
Atom positions and equivalent displacement factors for $Na_{1.2}V_3O_8$ and $Na_{0.7}Li_{0.7}[V_3O_8]$

	$Na_{1.2}V_3O_8$					$Na_{0.7}Li_{0.7}[V_3O_8]$			
	X	Y	Z	U[eq][a]		X	Y	Z	U[eq][a]
V(1)	0.1792(2)	0.25	0.0409(1)	0.0070(5)		0.1833(3)	0.25	0.0402(1)	0.0105(7)
V(2)	0.6029(2)	0.75	0.4195(1)	0.0086(5)		0.6132(3)	0.75	0.4220(1)	0.0111(7)
V(3)	0.2325(2)	0.25	0.3102(1)	0.0100(5)		0.2326(3)	0.25	0.3073(1)	0.0115(7)
O(1)	–0.0987(9)	0.25	–0.0391(5)	0.011(1)		–0.103(1)	0.25	–0.0405(6)	0.017(2)
O(2)	0.0117(9)	0.25	0.2360(5)	0.017(1)		0.007(1)	0.25	0.2300(7)	0.018(2)
O(3)	0.3053(8)	0.75	0.3284(5)	0.011(1)		0.307(1)	0.75	0.3278(6)	0.014(2)
O(4)	0.3382(8)	0.25	0.1757(5)	0.009(1)		0.348(1)	0.25	0.1757(6)	0.011(2)
O(5)	0.8056(9)	0.75	0.5382(5)	0.013(1)		0.819(1)	0.75	0.5408(7)	0.019(2)
O(6)	0.5314(9)	0.25	0.4274(5)	0.010(1)		0.537(1)	0.25	0.4290(6)	0.016(2)
O(7)	0.6880(9)	0.75	0.3111(5)	0.017(1)		0.705(1)	0.75	0.3153(7)	0.028(2)
O(8)	0.3089(8)	0.25	–0.0457(5)	0.012(1)		0.314(1)	0.25	–0.0476(7)	0.020(2)
M(1)	0.6657(5)	0.25	0.1741(3)	0.0173(9)		0.66970(9)	0.25	0.1755(5)	0.014(2)
M(2A)	0.995(2)	0.25	0.558(2)	0.033(8)[b]	$M(2)_{Fourier}$	0.926(1)	0.75	0.532(8)	0.02(2)[b,c]
					$M(3)_{Fourier}$	0.78(1)	0.25	0.49(1)	0.02(2)[b,c]

[a] U[eq] = $1/3(U_{11}^C + U_{22}^C + U_{33}^C)$ [31].
[b] Isotropic displacement factors.
[c] Constrained to be equal.

Table 3
Bond lengths [Å] in $Na_{1.2}[V_3O_8]$ and $Na_{0.7}Li_{0.7}[V_3O_8]$

	$Na_{1.2}[V_3O_8]$	$Na_{0.7}Li_{0.7}[V_3O_8]$		$Na_{1.2}[V_3O_8]$	$Na_{0.7}Li_{0.7}[V_3O_8]$
V(1)–O(8)	1.614(6)	1.598(9)	*M*(1)–O(4)	2.407(7)	2.285(10)
V(1)–O(4)	1.703(5)	1.721(7)	*M*(1–O(2)j	2.421(7)	2.30(1)
V(1)–O(1)a	1.896(2)	1.895(3)	*M*(1)–O(7)	2.425(5)	2.438(7)
V(1)–O(1)c	1.896(2)	1.895(3)	*M*(1)–O(7)e	2.425(5)	2.438(7)
V(1)–O(1)	1.978(6)	1.985(9)	*M*(1)–O(8)b	2.427(4)	2.401(7)
⟨V(1)–O⟩	1.817(4)	1.819(5)	*M*(1)–O(8)d	2.427(4)	2.401(7)
			⟨M(1)–O⟩	2.422 (5)	2.377(8)
V(2)–O(7)	1.616(6)	1.602(9)			
V(2)–O(5)	1.733(6)	1.731(8)	*M*(2)–O(5)f	2.13(2)	2.23(11)
V(2)–O(6)	1.889(2)	1.893(3)	*M*(2)–O(5)h	2.24(1)	1.97(4)
V(2)–O(6)l	1.889(2)	1.893(3)	*M*(2)–O(5)g	2.24(1)	1.97(4)
V(2)–O(3)	2.132(6)	2.149(8)	*M*(2)–O(7)f	2.39(2)	2.74(10)
V(2)–O(6)f	2.348(6)	2.344(9)	*M*(2)–O(3)	2.92(2)	2.68(10)
⟨V(2)–O⟩	1.935(5)	1.935(6)	M(2)–O(6)g	3.29(2)	2.68(10)
			⟨M(2)–O⟩	2.54(2)	2.38(8)
V(3)–O(2)	1.600(6)	1.606(8)			
V(3)–O(3)	1.875(2)	1.877(2)			
V(3)–O(3)e	1.875(2)	1.877(2)	*M*(3)–O(6)		1.65(15)
V(3)–O(5)g	1.942(6)	1.973(8)	*M*(3)–O(5)		1.89(4)
V(3)–O(4)	2.006(6)	1.987(8)	*M*(3)–O(5)g		1.89(4)
V(3)–O(6)	2.228(6)	2.242(8)	⟨M(3)–O⟩		1.81(8)
⟨V(3)–O⟩	1.921(5)	1.927(6)			

Equivalent positions: a: $-x, -y, -z$; b: $-x+1, -y, -z$; c: $-x, -y+1, -z$; d: $-x+1, -y+1, -z$; e: $x, y-1, z$; f: $x-1, y, z$; g: $-x+1, -y+1, -z+1$; h: $-x+1, -y+2, -z+1$; I: $x, y+1, z$; j: $x+1, y, z$.

Table 4
M-sites: average bond lengths [Å] and refined site occupancies

	M(1)	*M*(2)	*M*(3)
$Li_{1.2}[V_3O_8]$			
⟨M–O⟩ [Å]	$\langle^{[6]}$M–O$\rangle$ 2.207	$\langle^{[4]}$M–O$\rangle$ 2.01	—
Site populations	$Li_{1.0}$	$Li_{0.2}$	—
$Na_{1.2}[V_3O_8]$			
⟨M–O⟩ [Å]	11	2.3	—
	$\langle^{[6]}$M–O$\rangle$ 2.422(5)	$\langle^{[4]}$M–O$\rangle$ 2.25(2)	—
		$\langle^{[4+1]}$M–O$\rangle$ 2.38(2)	
		$\langle^{[4+2]}$M–O$\rangle$ 2.54(2)	
Site populations	$Na_{1.0}$	$Na_{0.21}$	$Na_{0.21(1)}$
$Na_{0.7}Li_{0.7}[V_3O_8]$			
⟨M–O⟩ [Å]	8.5	0.63	0.45
	$\langle^{[6]}$M–O$\rangle$ 2.377(8)	$\langle^{[3]}$M–O$\rangle$ 2.06(6)	$\langle^{[3]}$M–O$\rangle$ = 1.81(9)
		$\langle^{[3+3]}$M–O$\rangle$ 2.38(8)	
Site populations	$Na_{0.69(2)}Li_{0.31(2)}$	$Li_{0.21(6)}$	$Li_{0.15(6)}$
Chemical formula of NaLiV : $Na_{0.71}Li_{0.71}[V_3O_8]$			

The measured chemical composition of the NaLiV crystal is $Na_{0.71}Li_{0.71}[V_3O_8]$, in good agreement with the sum of the site populations derived from refinement of the crystal structure (Table 4).

3. Results and discussion

The structure refinements of NaV and NaLiV show that both structures have the same type of vanadate sheet as LiV, but they also indicate that the coordinations of the interstitial cations change across the $Na_xLi_y[V_3O_8]$ solid-solution.

3.1. Vanadate sheets in NaV and NaLiV

Hagenmuller reviewed the structures and chemical bonds in vanadium bronzes [35], Galy et al. [36] discussed the network architecture of lithium vanadates with the general formula $Li_xV_{3(1+n)}O_{8+7n}$, Evans and Hughes [24] classified natural and synthetic vanadium bronzes on the basis of different types of vanadate chains that are the fundamental

building blocks of the vanadate layers and Zavaliy and Whittingham [37] reviewed the structural chemistry of vanadium oxides with open frameworks.

Evans and Hughes [24] showed that the vanadate sheet in LiV is composed of alternately corner-shared tetravanadate and divanadate chains that extend parallel to the *b*-axis; i.e., parallel to the elongation of the crystals (also called the fibre axis). A tetravanadate chain contains four individual chains of dipyramids which join laterally by sharing inclined edges, forming a highly condensed $[V_4O_{12}]_n$ chain (indicated in black and light grey in Figs. 1–3). The $[V_2O_6]_n$ divanadate chain consists of two single chains of square pyramids which are joined laterally by sharing inclined pyramidal edges (indicated in dark grey in Figs. 1 and 2). The arrangement of the vanadate chains in the sheets of NaV, NaLiV and LiV is identical to the arrangement of chains in the sheets of the hydrous vanadate minerals of the hewettite group, $M_x^{z+}[V_6O_{16}](H_2O)_n$ (M^{z+} = Ca, Na_2) [25].

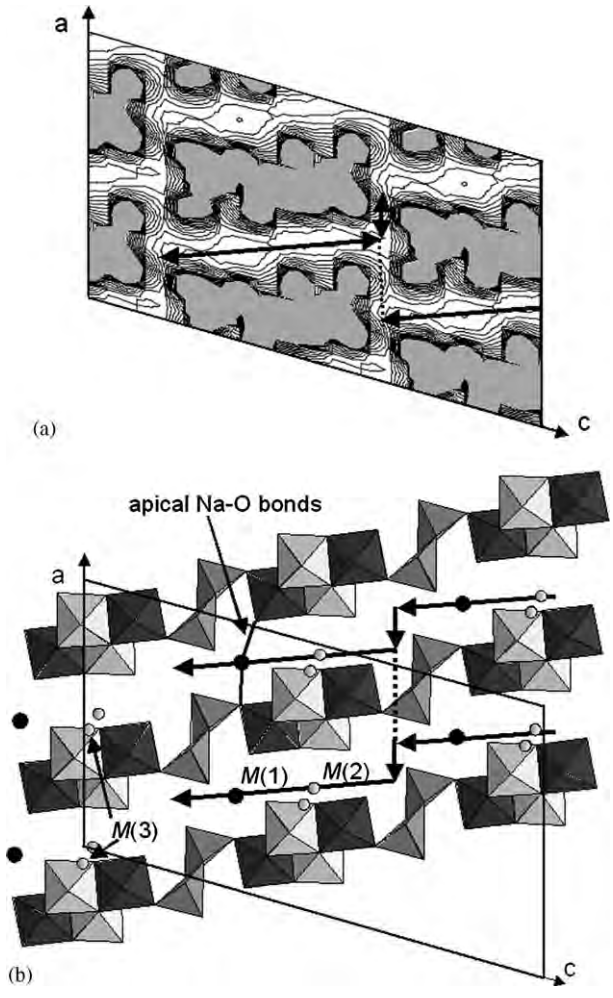

Fig. 2. (a) The bond-valence map for Li in the *ac*-plane at $y = 0.25$ of NaLiV, calculated with the bond-valence parameter for V^{5+} and containing 15 contour levels in an interval of 0.30 vu. (b) The structure of NaLiV in the same orientation as the bond-valence map. Black circles indicate octahedrally coordinated cations at the *M*(1) site and light grey circles indicate tetrahedrally coordinated cations at the *M*(2) site and trigonal coordinated cations at the *M*(3) site.

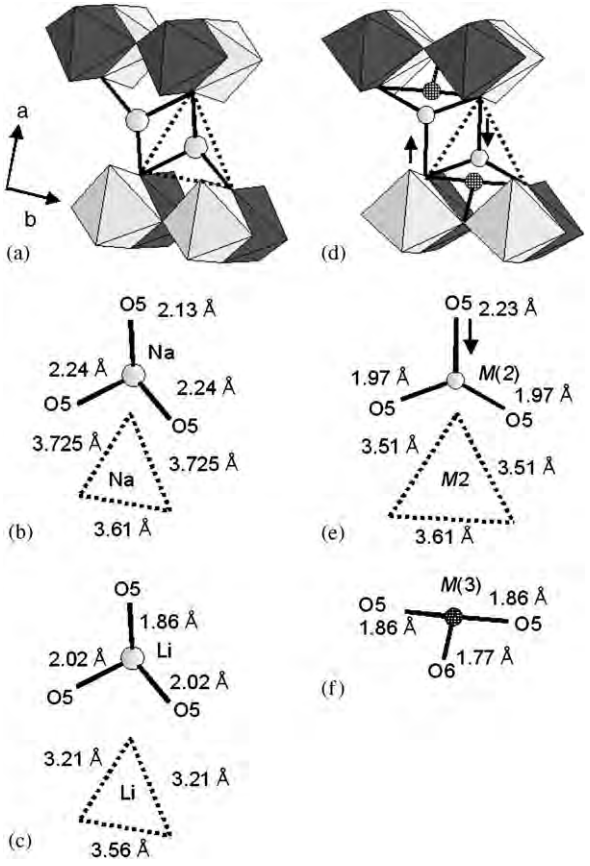

Fig. 3. (a) The *M*(2) site and the strong *M*(2)–O(5) bonds in the interlayer of NaV and LiV; the three *M*(2)–O(5) bonds form a triangle with the *M* cation in its center; selected interatomic distances in (b) NaV and (c) LiV; (d) the *M*(2) and *M*(3) sites in the interlayer of NaLiV and details of their coordination in (e) and (f) (see text for details).

Inspection of Table 3 shows that V(1) occurs in [5]-coordination, forming two shorter and three longer bonds with O-atoms. Schindler et al. [16] defined this type of coordination as a [2 + 3]-coordination, where the shorter vanadyl bonds are in the range 1.52–1.78 Å and the longer equatorial bonds are in the range 1.78 to >2.06 Å. The coordination of V(2) can be described as a [2 + 2 + 2]-coordination with two short vanadyl-, two equatorial- and two longer *trans* bonds (Table 2, [16]). Note that two vanadyl bonds always occur in the *cis*- (and never in the *trans*-) configuration [26]. The coordination of V(3) can be described as [1 + 4 + 1]-coordination with one short vanadyl-, four equatorial- and one longer *trans* bonds. Note that in Figs. 1–3, the V(2) and V(3) dipyramids are indicated in light grey and black, respectively.

In the structures of NaV and NaLiV, the average V(1)–O bond-length is 1.82 Å in close agreement with the average $^{[2+3]}V^{5+}$–O bond length in vanadates, 1.83 Å [16]. The average V(2)–O bond-lengths are 1.935 Å (NaV) and 1.927 Å (NaLiV), and are in close agreement with the average $^{[2+2+2]}V^{5+}$–O bond length in vanadates, 1.93 Å. The average V(3)–O bond lengths are 1.921 (NaV) and

1.927 Å (NaLiV), again close to the average $^{[1+4+1]}V^{5+}$–O bond length in vanadates, 1.93 Å [16].

The bond-valence tables for NaV, NaLiV and LiV are given in Tables 5–7. The parameters for V^{4+} and V^{5+} were taken from Brown and Altermatt [27]. Schindler et al. [16] showed that in V^{4+}-bearing compounds with polyhedra exclusively occupied by V^{4+}, V^{4+} occurs either in [1+4]- or [1+4+1]-coordination. For example, this is the case in $Li_4[V_3O_8]$ [10] in which V^{4+} occurs at all three V-sites in [1+4+1]-coordination. Note that during the lithation process of LiV, one O-atom shifts slightly toward V(1), resulting in a coordination change from [2+3] in $Li_{1.2}[V_3O_8]$ to [1+4+1] in $Li_4[V_3^{4+}O_8]$ [10].

The general coordination of V^{4+} suggests that in mixed valent V^{4+}/V^{5+} structures, V^{4+} should occur preferentially at sites at which the coordination of V is most similar to either [1+4] or [1+4+1]. Thus one would expect that in $M_{1+x}[V_3O_8]$ compounds ($x = 0.01$–1.00), V^{4+} should occur primarily at the V(3) site. This is indeed the case: the bond-valence sums calculated with the bond-valence curve for V^{5+} are lower at V(3) than at the V(1) and V(2) sites (Tables 5–7).

Schindler et al. [16] showed that one can determine the average valence of V, $\langle Z \rangle$, from the mean bond-length, $\langle R \rangle$, of the equatorial bonds in ($V^{4+/5+}O_n$) coordination polyhedra with V in [1+4]- and [1+4+1]-coordinations via the equation:

$$\langle Z \rangle = 28 - 12.50\langle R \rangle. \quad (1)$$

The mean $^{[1+4+1]}$V(3)–O equatorial bond-lengths are 1.925, 1.929 and 1.906 Å, and the resulting average charges at V(3) are 3.94 (NaV), 3.89 (NaLiV), and 4.18 (LiV) vu, respectively.

3.2. Coordination of the M sites in NaV

In the structure of NaV, Na(1) occurs in [6]-coordination at the $M(1)$ site (Table 3), which is sandwiched between the tetravanadate and divanadate chains of two adjacent vanadate layers (Fig. 2b). Na(2) occurs in [4]-coordination

Table 5
Bond-valence table for $Na_{1.2}[V_3O_8]$[a]

	V(1)	V(2)	V(3)	$M(1)$ $Na_{1.0}$	$M(2)$ $Na_{0.21}$	$\sum$
O(1)	$0.78^{\times 2}\rightarrow\downarrow$ (0.74) $0.62\downarrow\rightarrow$ (0.59)					2.18 (2.07)
O(2)			1.73 (1.64)	0.19		1.91 (1.82)
O(3)		0.41 (0.39)	$0.82^{\times 2}\rightarrow\downarrow$ $0.78^{\times 2}\rightarrow\downarrow$			2.05 (1.95)
O(4)	1.31 (1.24)		0.58 (0.55)	0.19		2.08 (1.98)
O(5)		1.21 (1.15)	0.69 (0.65)		0.08 $0.06^{\times 2}\rightarrow\downarrow$	2.10 (2.00)
O(6)		$0.79^{\times 2}\rightarrow\downarrow$ (0.75) 0.23 (0.22)	0.32 (0.30)			2.13 (2.02)
O(7)		1.66 (1.57)		$0.19^{\times 2}\rightarrow\downarrow$	0.04	2.08 (1.99)
O(8)	1.67 (1.58)			$0.18^{\times 2}\rightarrow\downarrow$		2.03 (1.94)
$\sum$	V^{5+}: 5.16 V^{4+}: (4.89)	V^{5+}: 5.09 V^{4+}: (4.78)	V^{5+}: 4.96 V^{4+}: (4.71)	1.12	0.21	

[a]Calculated bond-valences with the parameter for V^{4+} are given in parentheses. Bond-valence parameters are from Brown and Altermatt (1985).

Table 6
Bond-valence table for $Na_{0.7}Li_{0.7}[V_3O_8]$[a]

	V(1)	V(2)	V(3)	$M(1)$ $Na_{0.7}Li_{0.3}$	$M(2)$ $Li_{0.2}$	$M(3)$ $Li_{0.15}$	$\sum$
O(1)	$0.78^{\times 2}\rightarrow\downarrow$ (0.74) 0.61 (0.58)						2.17
O(2)			1.70 (1.62)	0.21			1.91 (1.83)
O(3)		0.39 (0.37)	$0.82^{\times 2}\rightarrow\downarrow$ (0.78)		0.01		2.04 (1.94)
O(4)	1.25 (1.18)		0.61 (0.58)	0.22			2.08 (1.98)
O(5)		1.22 (1.15)	0.63 (0.60)		0.05 $0.05^{\times 2}\rightarrow\downarrow$	$0.04^{\times 2}\rightarrow\downarrow$	2.08 (1.98)
O(6)		$0.78^{\times 2}\rightarrow\downarrow$ (0.75) 0.23 (0.22)	0.31 (0.29)		0.01	0.09	2.20 (2.11)
O(7)		1.72 (1.64)		$0.15^{\times 2}\rightarrow\downarrow$	0.01		2.03 (1.95)
O(8)	1.74 (1.65)			$0.16^{\times 2}\rightarrow\downarrow$			2.06 (1.97)
$\sum$	V^{5+}: 5.16 V^{4+}: (4.89)	V^{5+}: 5.12 V^{4+}: (4.87)	V^{5+}: 4.89 V^{4+}: (4.65)	1.05	0.16	0.19	

[a]Calculated bond-valences with the parameter for V^{4+} are given in parentheses. Bond-valence parameters are from Brown and Altermatt (1985).

Table 7
Bond-valence table for $Li_{1.2}[V_3O_8]$[a]

	V(1)	V(2)	V(3)	$M(1)$ Li_1	$M(2)$ $Li_{0.2}$	$\sum$
O(1)	$0.83^{\times 2}\rightarrow\downarrow$ (0.79) 0.64 (0.61)					2.30 (2.19)
O(2)			1.81 (1.72)	0.21		2.02 (1.93)
O(3)		0.45 (0.42)	$0.88^{\times 2}\rightarrow\downarrow$ (0.84)			2.21 (2.10)
O(4)	1.30 (1.23)		0.61 (0.58)	0.21		2.12 (2.02)
O(5)		1.32 (1.26)	0.69 (0.65)		$0.06\ 0.04^{\times 2}$6	2.15 (2.05)
O(6)		$0.85^{\times 2}\rightarrow\downarrow$ (0.81) 0.26 (0.25)	0.34 (0.32)			2.30 (2.19)
O(7)		1.78 (1.69)		$0.12^{\times 2}\rightarrow\downarrow$	0.03	2.05 (1.96)
O(8)	1.80 (1.71)			$0.13^{\times 2}\rightarrow\downarrow$		2.06 (1.97)
$\sum$	5.40 (5.13)	5.51 (5.24)	V^{5+}: 5.21 V^{4+}: (4.95)	0.93	0.17	

[a]Calculated bond-valences with the parameter for V^{4+} are given in parentheses. Bond-valence parameters are from Brown and Altermatt (1985).

at the $M(2)$ site (Table 3), which is located between two tetravanadate chains of two adjacent vanadate layers (Fig. 2b). Hence, the coordination of Na in NaV is identical to the coordination of Li in LiV. The mean $^{[6]}$Na–O and $^{[4]}$Na–O distances are 2.422(5) and 2.25(2) Å, and the effective ionic radii ($rO^{2-} = 1.40$ Å) of $^{[6]}$Na and $^{[4]}$Na are 1.022 and 0.85 Å, respectively. The radius of $^{[6]}$Na is in good agreement with the effective ionic-radius of $^{[6]}$Na, 1.02 Å, as reported by Shannon [29], while the radius of $^{[4]}$Na is much smaller than the effective ionic-radius of $^{[4]}$Na, 0.99 Å. However, Sokolova and Hawthorne [30] showed that in the well-refined structure of quadruphite, $Na_{14}Ca_2[Si_2O_7]_2(PO_4)_4O_4F_2$, the radius of $^{[4]}$Na can be as low as 0.89 Å, indicating that smaller radii than 0.99 Å do occur for $^{[4]}$Na. The atom O(3) is 2.92 Å from Na(2) and could be included in its coordination sphere (Table 3). However, the following two facts support a coordination number of [4] for Na(2):

(1) The V(2) site is 2.88 Å from Na(2) and therefore closer than O(3).
(2) The mean O–$^{[4]}$Na–O angle is 112° and is thus closer to the ideal tetrahedral angle of 109.5° than it is to the angles 100.0° and 90° for triangular-bipyramidal and square-pyramidal coordinations, respectively.

3.3. Site occupancy and coordination of the M sites in NaLiV

As the majority of the scattering occurs at the $M(1)$ site, it seems reasonable to assign all Na to this site (Na_xLi_{1-x}) assign Li to the $M(2)$ and $M(3)$ sites and refine the Li site-occupancies; the resultant values are given in Table 4, and are in reasonable accord with the composition derived from the chemical composition determined by LA-ICP-MS (Table 4).

In the structure of NaLiV, the mean $^{[6]}M(1)$–O bond length is 2.377 Å and the refined site-occupancy is $Na_{0.69}Li_{0.31}$. Assuming a linear correlation between the mean $M(1)$–O bond length and the amounts of Na and Li at the $M(1)$ site, the predicted mean $M(1)$–O bond length corresponding to this occupancy is $2.422 \times 0.69 + 2.207 \times 0.31 = 2.355$ Å, in reasonable agreement with the observed mean $M(1)$–O distance of 2.377 Å.

The cation(s) at the $M(2)$ site is in distorted [6]-coordination. There are three short bonds between 1.97 and 2.23 Å and three longer bonds between 2.68 and 2.74 Å. The cation(s) at the $M(3)$ site forms three very short bonds to adjacent O-atoms with a mean $M(3)$–O bond-length of 1.81(9) Å (Table 3). The $M(3)$ site is 2.19 Å from the V(2) site, which is closer than some O-atoms which are in the range 2.4–3.0 Å. Hence, the cation(s) at the $M(3)$ site are most likely in [3]-coordination, but an interaction between the cation(s) and the O-atoms at 2.4–3.0 Å cannot be ruled out.

3.4. M-site occupancies and the V^{4+}–V^{5+} ratio

The occupancies at the M sites show the chemical formulae of NaV and NaLiV to be $Na_{1.2}[V_3O_8]$ and NaLiV is $Na_{0.69}Li_{0.67}[V_3O_8]$, respectively (Table 4). The general composition $M_{1+x}[V_3^{5+}O_8]$ is electronically neutral where $x = 0$; additional interlayer cations ($x = 0.1$–1.0) must be charged–balanced by incorporation of V^{4+} at the V(3) site (see above). Hence, the interstitial charges of 1.2^+ in NaV and 1.4^+ in NaLiV require average V-charges at the V(3) site of 4.8^+ and 4.6^+, respectively. These charges are in reasonable accord with the bond-valence sums at the V(2) site, which were calculated on the basis of the bond-valence parameter for V^{4+}: 4.71 vu for NaV and 4.65 vu for NaLiV (Tables 5 and 6).

3.5. Interlayer distance between the vanadate sheets

Figs. 3a, d show parts of the bonding scheme of the interstitial cations at the $M(2)$ and $M(3)$ sites in NaV, LiV

and NaLiV. The cations at the $M(2)$ site (light grey circles) form three strong bonds to O(5), which are located in the tetravanadate chain linking two vanadate chains parallel to the b-axis. The cation(s) at the $M(3)$ site (cross-hatched circles) form three strong bonds to O-atoms in the same tetravanadate chains (Figs. 3d, f); some of the crystallographically identical $M(2)$ and $M(3)$ positions and weaker additional $M(2)$–O and $M(3)$–O bonds have been omitted for clarity. The three $M(2)$–O(5) bonds form a triangle in which the O(5)–$M(2)$–O(5) angles vary between 110 and 115° (Figs. 3a–d). The side of the triangle that connects two O(5) atoms in the same tetravanadate chain is parallel to the single vanadate chain (the b-axis). The length of the other two edges of the triangle may be used to express the distance between two tetravanadate chains.

Figs. 3b and c show that the distance between the O(5) atoms along the single vanadate chain is slightly larger in NaV than in LiV. However, the distance between O(5) atoms on opposite sides of the interlayer is much larger in NaV than in LiV (Figs. 3b, c). In NaLiV, the O(5)–O(5) distance along the vanadate chains is the same as in NaV, and the O(5)–O(5) distance across the interlayer is closer to the corresponding distance in NaV than in LiV. Closer inspection of Fig. 2b shows that the apical ligands of the $M(1)$ octahedra are located on two adjacent tetravanadate chains. Hence, the distance between two tetravanadate chains is also controlled by the size of the cation at the $M(1)$ site. Assuming a linear correlation between the site populations of Na and Li at $M(1)$ and the O(5)–O(5) distance across the interlayer, the predicted O(5)–O(5) distance in NaLiV is $3.725 \times 0.69 + 3.21 \times 0.31 = 3.56$ Å. This predicted value is reasonably close to the observed value of 3.51 Å in NaLiV, indicating that the interlayer distance between the tetravanadate chains is controlled by the occupancy of the $M(1)$ site.

The observed O(5)–O(5) distances in NaLiV have the consequence that Li becomes too small in the O(5)–O(5)–O(5) triangle and is forced to shift from the $M(2)$ position in LiV to the $M(2)$ or $M(3)$ positions in NaLiV (indicated with arrows in Figs. 3d, e). The positions of $M(2)$ and $M(3)$ are closer to one of the tetravanadate chains and are characterized by shorter M–O distances than those in LiV (Table 3).

Let us consider a short-range-order model in which all $M(1)$ sites in the vicinity of an $M(2)$ site are occupied by Na. In this case, the O(5)–O(5) distances across the interlayer would be larger than the average value of 3.51 Å. If this is the case, Li may be too small for the $M(2)$ site and will be forced to move to the $M(3)$ site. The difference-Fourier map indicates continuous electron-density between $M(2)$ and $M(3)$ (Fig. 1b), suggesting that Li may also occur between both sites. If this is the case, the $M(2)$ and $M(3)$ sites should be considered as two possible locations for Li; $M(2)$ is the position of Li where the tetravanadate chains are closest, and $M(3)$ is the position of Li where the tetravanadate chains are furthest away from each other.

4. Bond-valence maps

A bond-valence map can be used to explore the space available to an ion when most of the structure is known. The method was first proposed by Waltersson [38] who used it to find the sites of the Li ions in various Li_2WO_4 phases where the relatively weak scattering of the Li ion made it difficult to locate by X-diffraction. He placed a Li ion at an arbitrary point in the unit cell and calculated the lengths of the bonds it would form to the neighbouring O^{2-} ions. From these distances, he calculated the bond-valence sum around the Li ion using one of the following equations [28]:

$$S_{ij} = \exp[(R_0 - R_{ij})/B], \tag{2}$$

$$S_{ij} = (R_{ij}/R_0) - N, \tag{3}$$

where R_{ij} is the length of the bonds between atoms i and j, and S_{ij} is its experimental valence. R_0, B and N are parameters that are chosen to ensure that the sums of the bond valences around all the ions (cations as well as anions) in a large number of well-determined structures are the same as their atomic valences (formal charges). The Li ion was then moved to other positions in the cell and the calculation repeated to generate a map of the incident bond-valence sum that a Li ion would have if placed at any given point in the crystal.

In this paper, the bond-valence maps with respect to the interstitial cations Na and Li were calculated with the program VALMAP 2.0 [34]. The program calculates the bond-valence sum $\sum s_i$ that a particular atom would have if it were placed at any arbitrary point in the crystal. The program moves the atom systematically through all points of a selected grid (usually $25 \times 25 \times 25$) and maps the bond-valence sum for the specific cation (or anion) under consideration. Maxima in the contour map represent the atoms of the structure and minima indicate potential sites with valences equal to the bond-valence sum, respectively. The number and range of contour levels can be modified in order to focus on a particular zone of the map. One can use different bond-valence equations and different values for the empirical parameter R_0 and b (for details, see Brown, [28])

We have calculated the bond-valence sum for the interstitial cations Na and Li in NaLiV, NaV and LiV in order to map:

(a) The contour line representing the bond-valence sum of 1 vu (or as close as possible).
(b) Features such as interstitial area, vanadate polyhedra and *diffusion pathways* through the interstitial area.

It must be emphasized that although the structure type of the phases of the $Li_{1-x}Na[V_3O_8]$ solid solution is well known, one needs the atom positions of the specific phase of interest in order to calculate the bond-valence maps for the interstitial cations.

Figs. 2a, 4–7 show bond-valence maps for Li and Na in the structures of NaLiV, NaV, and LiV, the observed cation positions, and the calculated bond-valence sums for these positions. The bond-valence sum represented by each contour line is calculated manually using the atom positions given by VALPMAP [34] and the corresponding M–φ bond lengths calculated with SHELXTL-97 version [23]. The bond-valences are calculated with the bond-valence parameters for Na, Li and V^{5+} from Brown and Altermatt [27] and are listed with the coordinates of the observed positions in Table 8. Furthermore, we calculated other potential positions of Na and Li in these compounds, which are listed with their coordinates and bond-valence sums in Table 8.

4.1. Na–Li–$[V_3O_8]$ compounds

There are two different ways to calculate bond-valence maps for Na and Li in the Na–Li–$[V_3O_8]$ compounds. (1) One can include the bond-valence parameters for V^{5+}, which means that the calculated bond-valence sums include bond-valences of "Li–V bonds". These imaginary Li–V bonds greatly increase the bond-valence sums of Na and Li inside the vanadate polyhedra (where, of course, they cannot occur due to cation–cation repulsion). This has the advantage that the position of the vanadate polyhedra can be recognized in the contour plots, and it is easily apparent that Li will never move through these polyhedra. If the input file does not contain any information on V^{5+}, the contour plots show positions with a low bond-valence sum in the center of the vanadate polyhedra. In order to visualize the difference in appearance of the corresponding contour maps, we show the bond-valence maps for Li in NaLiV with and without any information on V^{5+} in Figs. 2a and 4, respectively.

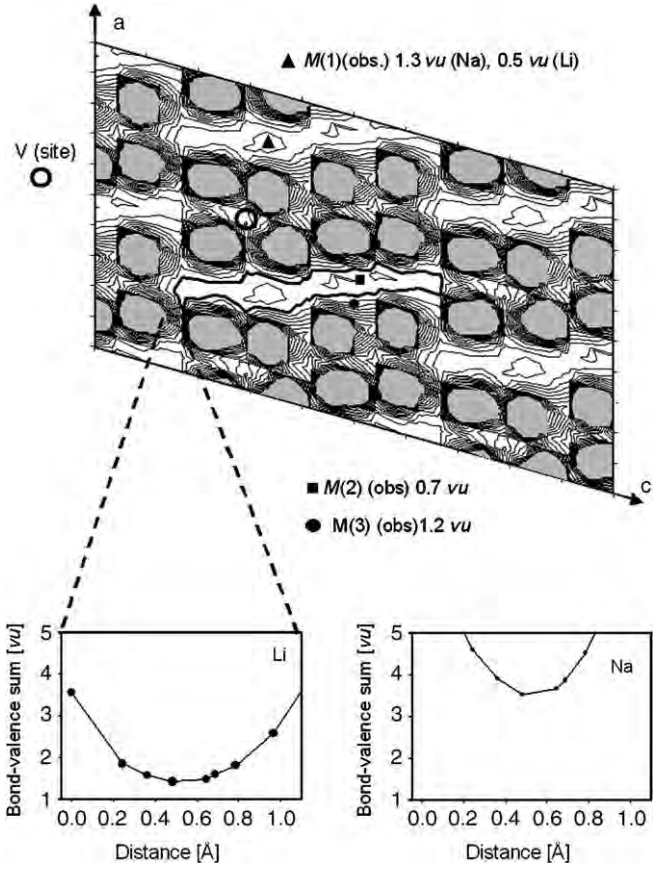

Fig. 4. (top) The bond-valence map for Li in the ac-plane at $y = 0.25$ of NaLiV, calculated without any information on V^{5+} and containing 15 contour levels with an interval of 0.30 vu; the contour line representing the bond-valence sum of 1.0 vu is marked with a thick black line. (bottom) Cross sections of the narrow pathways close to the divanadate chains, with the distance in the pathway plotted against the bond-valence sums for Li and Na.

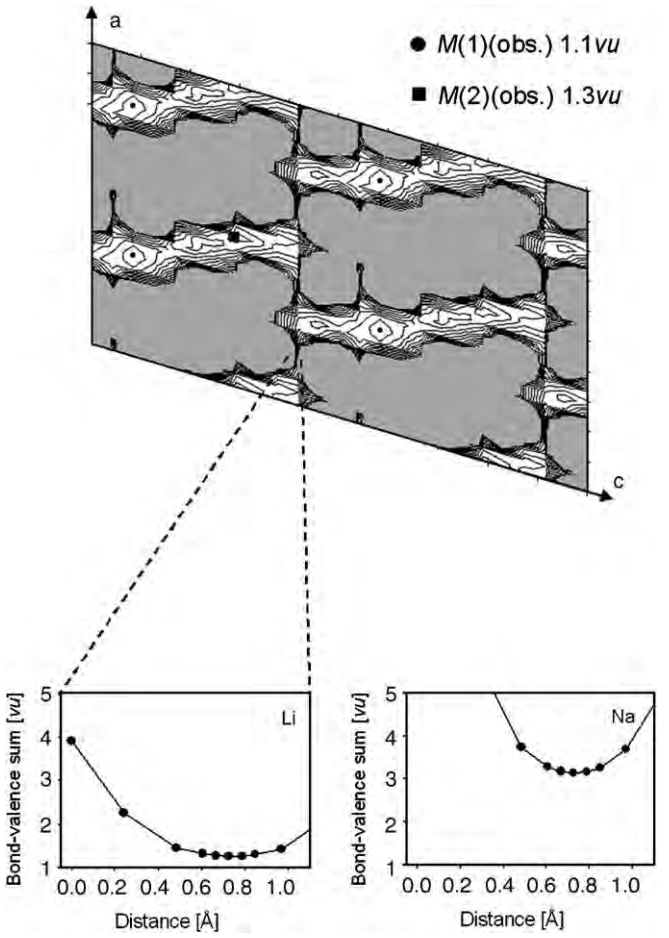

Fig. 5. (top) The bond-valence map for Na in the ac-plane at $y = 0.25$ of NaV, calculated without any information on V^{5+} and containing 15 contour levels with an interval of 0.35 vu; the first contour line represents the bond-valence sum of 1.1 vu. (bottom) Cross sections of the narrow pathways close to the divanadate chains, with the distance along the pathway plotted against the bond-valence sums for Li and Na.

Fig. 2a shows the bond-valence map for Li in NaLiV. The contour plot shows the bond-valence sums in the ac-plane at a height of $y = 0.25$. All atoms in the structure of NaLiV lie on this plane (x, 0.25, z) (Table 2), which corresponds to the mirror parallel to the ac-plane. The bond-valence map was calculated with the bond-valence parameter for V^{5+}, considering only Li–φ bonds up to 3 Å

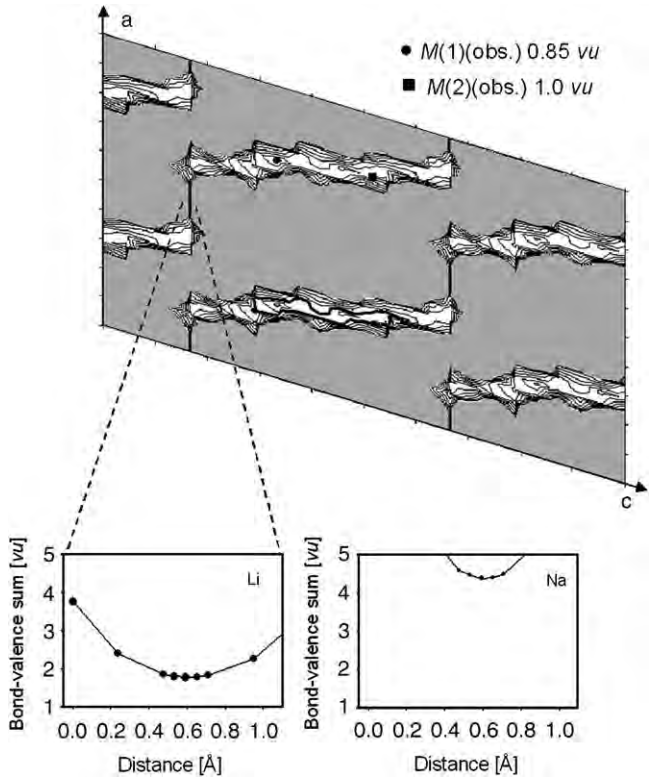

Fig. 6. (top) The bond-valence map for Li in the *ac*-plane at $y = 0.25$ of LiV, calculated without any information on V^{5+} and containing 15 contour levels with an interval of 0.07 vu; the first contour line represents the bond-valence sum of 0.9 vu and the contour line representing 1.0 vu is marked with thick black line. (bottom) Cross sections of the narrow pathways close to the divanadate chains, with the distance in the pathway plotted against the bond-valence sums for Li and Na.

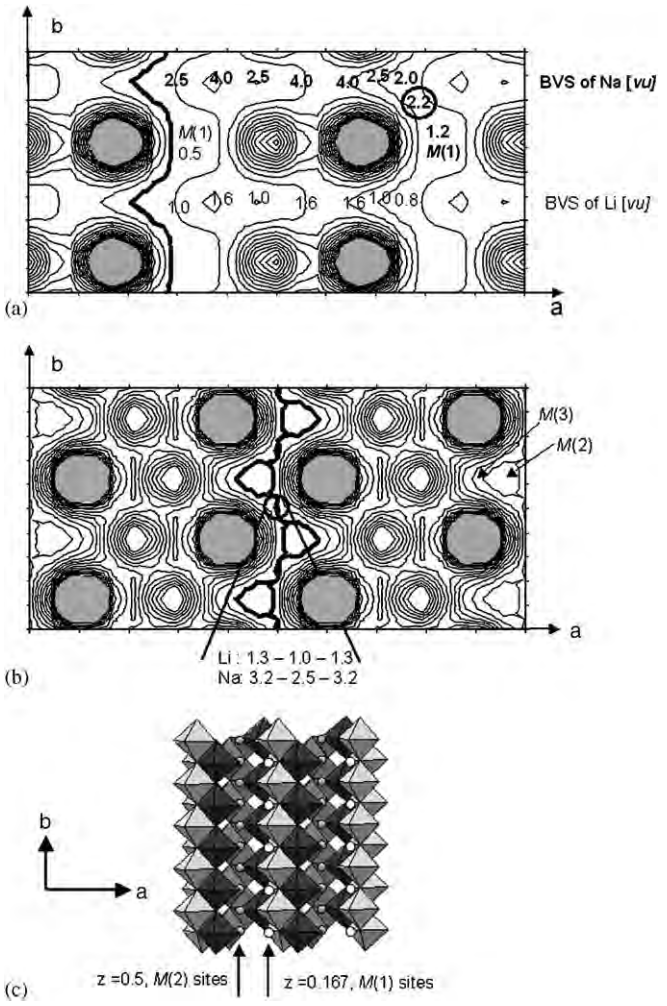

Fig. 7. (a)–(b) Bond-valence maps for Li in NaLiV in the *bc*-plane at heights of (a) $z = 0.17$ (level of $M(1)$ in z) and (b) $z = 0.5$ (level of $M(2)$ in z), calculated without any information on V^{5+} and containing 15 contour levels with an interval of (a) 0.60 and (b) 0.30 vu. Contour lines representing the bond-valence sum of 1.0 vu are marked with thick black lines. The bond-valence sums for Li and Na are indicated in normal and bold letters, respectively. (c) The structure of NaLiV in the orientation of the bond-valence maps [for clarity without $M(3)$]. The locations of the $M(1)$ and $M(2)$ sites at different z are indicated with arrows.

(φ = O, V), and using 15 contour levels with an interval of 0.3 vu. Fig. 2b indicates the orientation of the map with respect to the sheet of polymerized vanadate polyhedra. The locations of the vanadate polyhedra in the contour plot appear black, because the bond-valence sums at these positions are high (>4.5 vu). The areas of potential Li positions contain contour lines indicating minima in the bond-valence sum. These areas are indicated with long arrows extending along the elongation of the interstitial areas, and may be described as *bond-valence or diffusion pathways* in which the interstitial cations can move without major deviations from their bond-valence requirements. These pathways narrow and bifurcate close to the divanadate chains: one of the pathways remains inside the interstitial area (indicated with a small arrow), whereas the other pathway passes through a vanadate pyramid (indicated with dashed lines).

Figs. 4–7 show bond-valence maps for Li and Na in NaLiV, NaV and LiV in the *ac*-plane at $y = 0.25$ and in the *bc*-plane at $z = 0.17$ and $z = 0.5$. They were calculated without any information on V^{5+} and the bond-valence sums were calculated for Li–O and Na–O bonds up to 3.0 Å. The bond-valence map in Fig. 6 was calculated with a small interval between the contour levels for the better visualization of the potential pathways of the interstitial cations in the *ac*-plane of LiV.

4.2. Additional positions for Na and Li

Potential positions of monovalent cations in the interlayer of the Na–Li vanadates are indicated by the 1.0 vu (or very close to 1.0 vu) contour line. De Picciotto et al. [10] showed that the structure of $Li_4[V_3O_8]$ can be described as an almost cubic-close packing of O-atoms, in which the V and Li atoms occur at the octahedral sites. These octahedral sites occur in layers at the special position (x, 0.25, z), which seems most likely the potential space of other cation positions.

In the bond-valence maps for Li in NaLiV and LiV, the 1.0 vu contour lines are indicated as thick black lines

Table 8
Observed and additional calculated M-positions in $M_x[V_3O_8]$ compounds (M = Na, Li) and the bond-valence sums of the M-cations ($\sum s$)[a]

	X	Y	Z	$\sum$s [vu]
$Na_{0.7}Li_{0.7}[V_3O_8]$				
$M1$ (obs)	0.6697	0.25	0.1755	1.3 (Na)/0.5 (Li)
$M2$ non-splitted (obs)	0.91	0.25	0.52	0.7 (Li)
$M2$ (obs)	0.926	0.25	0.532	0.7 (Li)
$M3$ (obs)	0.78	0.25	0.49	1.2 (Li)
$M4$(calc)	−0.472	0.25	−0.190	1.0 (Li)
$M5$(calc)	0.083	0.25	0.748	1.0 (Li)
$M6$(calc)	−0.208	0.25	0.448	1.0 (Li)
$M7$(calc)	0.058	0.25	0.84	1.0 (Li)
$Li_{1.2}[V_3O_8]$				
$M1$(obs)	0.501	0.25	0.683	0.9
$M2$ (obs)	0.57	0.25	0.050	1.0
$M3$(calc)	0.583	0.25	−0.079	1.0
$M4$(calc)	0.585	0.25	0.079	1.0
$Na_{1.2}[V_3O_8]$				
$M1$ (obs)	0.6657	0.25	0.174	1.1
$M2$ (obs)	0.995	0.25	0.558	1.3
$M3$(calc)	−0.084	0.25	0.452	1.3
$M4$(calc)	0.583	0.25	−0.081	1.7
$M5$(calc)	−0.501	0.25	−0.167	1.7

[a]Bond-valence parameter are from Brown and Altermatt (1985).

(Figs. 4 and 7). For both structures, potential positions for Li occur along these contour lines; selected positions are listed in Table 8. The Li atoms at these positions are usually coordinated by three or four O-atoms at distances of 1.75–2.3 Å and by two to four additional O-atoms at distances of 2.3–3.0 Å. It is notable that the 1.0 vu contour line occurs between the $M(2)$ and $M(3)$ sites (Fig. 4), confirming our suggestion above that Li may also occur between these sites, depending on the occurrence of Na or Li at the $M(1)$ site.

In the bond-valence map for Na in NaV, there is only one point (1.1 vu) with a bond-valence sum close to 1.0 (indicated as a black circle in Fig. 5). Additional calculated positions for Na never resulted in bond-valence sums close to 1.0 vu; positions representing the lowest bond-valence sums of 1.3 and 1.7 vu are listed in Table 8.

4.3. Diffusion pathways versus electrochemical performance

Kumagai et al. [9] examined the $Li_{1-x}Na[V_3O_8]$ solid-solution as a positive material for secondary lithium batteries and found that $Li_{0.7}Na_{0.3}[V_3O_8]$ showed the best electrochemical performance regarding discharge capacity and chemical-diffusion coefficient. They proposed that the larger Na cation produces a weaker interaction between the intercalated Li and the "host structure" so that substitution of Li by Na in $Li[V_3O_8]$ leads to "a decrease in the site energies available to the incorporated Li atoms". Furthermore, they showed that in a $Li_n/Li_{0.7}Na_{0.3}[V_3O_8]$ cell, intercalation of additional Li does not displace any Na, and suggested that the Na atoms are firmly bound to the oxide matrix.

The calculated bond-valence maps (Figs. 4–7) enable us to explain the observed diffusion properties of Li and Na in the $Li_{1-x}Na[V_3O_8]$ solid-solution. In order to do so, we need to examine the bond-valence sums for Li and Na that occur in the bond-valence pathways in the interlayer of the vanadate sheets; i.e., one can either inspect the contour levels representing the valence of the cation or one can calculate cross-sections perpendicular to the orientation of the pathways close to the divanadate chains. Cross sections were calculated for Li and Na in NaLiV, NaV and LiV (Figs. 4–7). The bond-valence sums for both cations are either shown as a function of position inside the pathway [the origin is on the left and the endpoint is on the right, Figs. 4–6)] or indicated on the corresponding contour lines (Figs. 7a, b). Before we evaluate the pathways for each cation, we must define a range of bond-valence sums at which the bond-valence requirements of the cation are reasonably well-satisfied. On the basis of our experience, calculated bond-valence sums in the range 0.7–1.3 vu for alkaline cations are quite common, and this range may be used to evaluate possible pathways for diffusion.

Closer inspection of the bond-valence maps for Li in LiV and Na in NaV (Figs. 4 and 5) shows that Li can move over much of the interstitial space, whereas Na is restricted to smaller regions. Furthermore, the bond-valence sums for Na in the narrow pathways of NaLiV, NaV and LiV never drops below 3 vu and indicates no diffusion of Na along these channels. However, the minimum bond-valence sums for Li in these narrow pathways are 1.3, 1.4 and 1.8 vu for NaV, NaLiV and LiV, respectively. Furthermore, the bottoms of the pathways narrow with increasing amount of Li in the structure. These observations suggest that

(a) Diffusion of Li through these narrow pathways is promoted by the interstitial space between adjacent vanadate chains.
(b) The diffusion of the cation along this pathway may not be significant in the structure of LiV.
(c) The interstitial space in which the bond-valence sums for Li are close to its valence increases with the amount of Na in the structure.

Let us consider next the potential diffusion pathways in the bond-valence maps drawn in the *ab*-plane (Figs. 7a and b). Pathways in these planes are important because the $M(1)$ and $M(2)$ sites occur in the structures of NaV, NaLiV and LiV, resulting in rows of cations parallel to the *b*-axis. These rows may be an indication of a possible diffusion path in this direction because of the short interval of potential cation positions along the path. Inspection of the bond-valence maps shows that this may indeed be the case: 1.0 vu contour lines extend parallel to rows of cations; i.e., parallel to the divanadate and tetravanadate chains and the fiber axis of the crystal. Figs. 7a and b show that parallel to

this contour line, the minimum bond-valence sums for Na are at $z = M(1)$: 1.2 (at the $M(1)$ site), 2.0 and 2.2 vu and at $z = M(2)$: 2.5 vu, indicating again that diffusion of Na along this path is unlikely in NaLiV.

Inspection of the bond-valence maps for Li in LiV and for Na in NaV show that the bond-valence sums at the positions indicated with circles in Figs. 7a and b are 1.3 at $z = M(1)$ and 1.5 vu at $z = M(2)$ for Li, and 2.0 at $z = M(1)$ and 1.8 vu at $z = M(2)$ for Na. These values show again that the bond-valence sums for Li along the pathways in LiV are always higher than the corresponding values in NaLiV, and that the bond-valence potential for Na in NaV is often far too high for diffusion of Na along these pathways. Fig. 7a shows that there is a potential diffusion pathway for Li parallel to a at $z = 0.17$ and $y = 0.75$. However, the maximum bond-valence sum along this pathway is 1.6 vu, which may indicate only limited diffusion of Li in this direction.

4.4. Diffusion versus temperature

Figs. 4–7 show that along diffusion pathways, the bond-valence sum for Na and Li depends on the distance between the vanadate polyhedra along the path. For example, the diffusion pathway for Li in the *ac*-plane of NaLiV is parallel to the 1.0 vu contour line until the pathway closely approaches the divanadate chains where the bond-valence sum for Li increases to 1.3 vu (Fig. 4). Another example are the diffusion pathways for Li in the *ab*-plane at $z = M(1)$ and $M(2)$ in NaLiV. Here, the pathways parallel to the *b*-axis follow the 1.0 vu contour line, whereas bond-valence sums for Li increases and decreases from 0.8 to 1.6 vu along the diffusion pathway parallel to the *a*-axis. If we consider the effect of temperature, the diffusion of Li atoms along the 1.0 vu contour-line should be more or less independent of temperature because there are no bond-valence barriers along the pathway. The situation is different along pathways with high and low bond-valence sums for Li. The fluctuation in the bond-valence sum with position suggests hopping of Li between positions with bond-valence sums close to 1.0 vu. In such a case, the higher kinetic energy of Li atoms at higher temperature will promote such hopping between positions where the bond valence is approximately 1.0 vu. Hence with increasing temperature, there should be increased diffusion of Li parallel to the *a*-axis in the *ab*-plane of NaLiV (at $z = M(1)$, Fig. 7a) and in the interstitial area in the *ac*-plane of NaLiV (at $y = 0.25$, Fig. 4).

We can summarize the potential bond-valence paths for Li and Na in NaLiV, NaV and LiV as follows:

1. There are uninterrupted 1.0 vu contour lines of Li bond-valence potential parallel to the fibre axis and extending through the $M(1)$ and $M(2)$ sites.
2. The maximum bond-valence sums for Li at corresponding positions along the diffusion pathways are always smaller in NaV than in NaLiV, and smaller in NaLiV than in LiV.
3. The bond-valence sums for Na along potential pathways in NaLiV, NaV and LiV indicate that the bond-valence requirements of Na are far from being satisfied, and hence Na will not diffuse to any significant amount.
4. Diffusion pathways with significant fluctuations in the bond-valence sum for Na^+ and Li^+ may be promoted by higher temperature, because the higher kinetic energy of the cations at higher T should promote hopping between positions with ideal bond-valence sums.

These results confirm the proposal of Kumagai et al. [9] that the larger interstitial space in Na-rich structures decreases the interaction between Li and the "host structure". Our results and the results of Kumagai et al. [9] suggest that the amount of Li and the bond-valence potential of Li in the interstices are the most important factors affecting the diffusion coefficient of Li in $Li_n/Li_{0.7}Na_{0.3}[V_3O_8]$ cells. If this is the case, the chemical compositions with the best diffusion coefficients in other solid-solution series can be determined via calculation of bond-valence maps. Here, the optimum diffusion coefficient of the smaller cation A in the A/A_xB_{1-x} [structural unit] cells should occur at the highest possible value of x, where uninterrupted 1.0 vu contour lines of bond-valence potential of cation A still occur in the interstices. In this way, optimum diffusion coefficients of cations may be found through structural characterization of the ion-conductor in a solid-solution series and calculation of the corresponding bond-valence maps for the interstitial cations.

5. Summary

Refinement of the structure of $Na_{1.2}[V_3O_8]$ (NaV) shows that the octahedrally coordinated $M(1)$ site is fully occupied by Na, and the [4]- or [5]-coordinated $M(2)$ site is partly occupied by Na. The $M(1)$ site is located between tetravanadate and divanadate chains and the $M(2)$ site is sandwiched between two tetravanadate chains. Both sites are identical to the Li sites in $Li_{1.2}[V_3O_8]$ (LiV). Refinement of the structure of $Na_{0.7}Li_{0.7}[V_3O_8]$ (NaLiV) shows that

(1) Na and Li occur at the $M(1)$ site, with site occupancies of 0.69 and 0.31, respectively.
(2) The $M(2)$ site is split into an $M(2)$ site and an $M(3)$ site, both of which are located closer to the vanadate layers than the $M(2)$ site in NaV and LiV.
(3) Li occurs at the $M(2)$ and $M(3)$ sites, indicating preferred incorporation of Li in the interlayer of the tetravanadate chains.
(4) The occupancy at the $M(1)$ site results in a larger distance between the tetravanadate chains than is the case in LiV. As a consequence, interstitial Li is forced to move toward one of the tetravanadate chains. The occurrence of Li at either $M(2)$ or $M(3)$ may depend on the composition of the adjacent $M(1)$ sites.

(5) Calculation of bond-valence maps for Li and Na show the occurrence of alternative positions at which the bond-valence sum of the cation is close to being satisfied.
(6) Calculation of bond-valence maps for Na and Li in NaLiV, NaV and LiV explain some previous observations of electrochemical performance of Na–Li–$[V_3O_8]$ solid solutions [9]. Furthermore, the bond-valence maps for Li indicate the diffusion paths for Li parallel to the fibre axis of the crystal.

Acknowledgments

We thank Mark Cooper for assistance on the single-crystal X-ray diffractometer and Lucy Rajnovic and Shawna McCright for discussions. FCH was supported by NSERC through a Canada Research Chair in Crystallography and Mineralogy, and Research Tools and Equipment, Discovery and Major Facilities Access grants.

References

[1] F. Bonino, M. Ottaviani, B. Scrosati, G. Pistoia, J. Electrochem. Soc. 135 (1988) 12–15.
[2] A. Hammou, Aa. Hammouche, Electrochim. Acta 33 (1988) 1719–1720.
[3] M. Pasquali, G. Pistoia, V. Manev, R.V. Moshtev, J. Electrochem. Soc. 133 (1986) 2454–2458.
[4] G. Pistoia, M. Pasquali, M. Tocci, V. Manev, R.V. Moshtev, J. Power Sources 15 (1985) 13–25.
[5] G. Pistoia, M. Pasquali, M. Tocci, R.V. Moshtev, V. Manev, J. Electrochem. Soc. 132 (1985) 281–284.
[6] G. Pistoia, S. Panero, M. Tocci, R.V. Moshtev, V. Manev, Solid State Ion. 13 (1984) 311–318.
[7] K. Nassau, D.W. Murphy, J. Non-Cryst. Solids 44 (1981) 297–304.
[8] I.D. Raistrick, Rev. Chim. Miner. 21 (1984) 456–467.
[9] N. Kumagai, A. Yu, K. West, J. Appl. Electrochem. 27 (1997) 953–958.
[10] L.A. de Picciotto, K.T. Adendorff, D.C. Liles, M.M. Thackeray, Sold State Ion. 62 (1993) 297–307.
[11] M. Pasquali, G. Pistoia, Electrochim. Acta 36 (1991) 1549–1553.
[12] G. Pistoia, G. Wang, D. Zane, Solid State Ion. 76 (1985) 285–290.
[13] P. Novak, W. Scheifele, F. Joho, O. Haas, J. Electrochem. Soc. 142 (1995) 2544–2550.
[14] G. Wang, G. Pistoia, J. Electroanal. Chem. 302 (1991) 275–278.
[15] A.D. Wadsley, Acta Crystallogr. 10 (1957) 261–267.
[16] M. Schindler, F.C. Hawthorne, W.H. Baur, Chem. Mater. 12 (2000) 1248–1259.
[17] M. Schindler, F.C. Hawthorne, W.H. Baur, Can. Mineral. 38 (2000) 1443–1456.
[18] M. Schindler, F.C. Hawthorne, J. Solid State Chem. 146 (1999) 271–276.
[19] J.M. Hughes, M. Schindler, J. Rakovan, F. Cureton, Can. Mineral. 40 (2002) 1429–1435.
[20] J.M. Hughes, M. Schindler, C.A. Francis, Can. Mineral. 43 (2005) 1379–1387.
[21] G.M. Sheldrick, SADABS User Guide, University of Göttingen, Germany, 1996.
[22] J.A. Ibers, W.C. Hamilton (Eds.), International Tables for X-Ray Crystallography IV, Kynoch Press, Birmingham, UK, 1974.
[23] SHELXTL NT, Program Suite for Solution and Refinement of Crystal Structures, Version 5.1, Bruker Analytical X-ray Systems, Madison, WI, 1998.
[24] H.T. Evans Jr., J.M. Hughes, Am. Miner. 75 (1990) 508–521.
[25] H.T. Evans Jr., Can. Miner. 27 (1989) 181–188.
[26] H.T. Evans Jr., Z. Kristallogr. 114 (1960) 257–277.
[27] I.D. Brown, D. Altermatt, Acta Crystallogr. B 41 (1981) 244–247.
[28] I.D. Brown, in: M.O. Keeffe, A. Navrotsky (Eds.), Structure and Bonding in Crystals II, vol. 1B, Academic Press, New York, 1981, pp. 1–30.
[29] R.D. Shannon, Acta Crystalllogr. A 32 (1976) 751–761.
[30] E. Sokolova, F.C. Hawthorne, Can. Mineral. 39 (2001) 1275–1299.
[31] W.C. Hamilton, Acta Crystallogr. 12 (1959) 609–610.
[32] N.J.G. Pearce, W.T. Perkins, J.A. Westgate, M.P. Gorton, S.E. Jackson, C.R. Neal, S.P. Chenery, Geostandards Newslett. 21 (1997) 115–144.
[33] E. van Achterberg, C.G. Ryan, W.L. Griffin, GLITTER Version 4 On line Interactive Data Reduction for the LA-ICPMS Microprobe, Macquarie Research Ltd., 2001.
[34] J. Gonzáles-Platas, C. Gonzáles-Silgo, C. Ruiz-Pérez, J. Appl. Crystallogr. 32 (1999) 341–344.
[35] P. Hagenmuller, Cryst. Struc. Chem. Bond. Inorg. Chem. 1 (1975) 69–82.
[36] J. Galy, J.-M. Savariault, C. Roucau, Aust. J. Chem. 49 (1996) 1009–1018.
[37] P.Y. Zavalij, M.S. Whittingham, Acta Crystallogr. B 55 (1999) 627–663.
[38] K. Waltersson, Acta Crystallogr. A 34 (1978) 901–905.